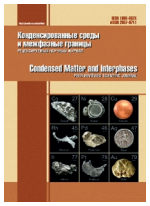

ISSN 1606-867X (Print)
ISSN 2687-0711 (Online)
Condensed Matter and Interphases
Kondensirovannye Sredy i Mezhfaznye Granitsy
https://journals.vsu.ru/kcmf/

Original articles

Research article
https://doi.org/10.17308/kcmf.2022.24/10559

Modelling optical polarization processes on laser modified titanium with a polyvinyl alcohol film

A. V. Tsibulnikova[1]✉, A. A. Khankaev[1], D. A. Artamonov[1], I. G. Samusev[1], V. A. Slezhkin[2], I. I. Lyatun[1], V. V. Bryukhanov[1]

[1]*Immanuel Kant Baltic Federal University,*
14 A. Nevskogo ul., Kaliningrad 236016, Russian Federation

[2]*Kaliningrad State Technical University,*
1 Sovetsky pr., Kaliningrad 236022, Russian Federation

Abstract

The article presents the results of research of optical spectra of surface plasmon polaritons on laser modified titanium with a deposited micron polymer polyvinyl alcohol (PVA) film.

The metasurface of titanium was created by means of femtosecond laser treatment with λ = 1.035 μ and the duration τ = 280 fs with linear and circular radiation polarization. Sets of laser pulses were applied pointwise to the surface with a step of 100 μm with the interval t_i = 25–750 ms. In the case of linear radiation polarization, tracks of ripple structures with a line density of up to N ~ 1,200 mm^{-1} appeared on the scribed titanium surface. It was found that when titanium is exposed to circular polarization radiation, occasional ablation cavities with lobed circular ripple nano-microstructures appear along the line of beam pulse propagation.

Mathematical modelling of real Re(ε) and imaginary Im(ε) permittivity established that the spectral parameters in the reflectance spectra of polarized radiation almost fully matched. The analysis of the spectra also established that the maximum absorption was in the IR region due to the presence of a PVA film.

Keywords: Plasmon resonance, Laser structuring, Circular polarisation, Metasurface, PVA film

Funding: The study received financing within the framework of project No. FZWM-2020-0003 supported by the Ministry of Science and Higher Education.

For citation: Tsibulnikova A. V., Khankaev A. A., Artamonov D. A., Samusev I. G., Slezhkin V. A., Lyatun I. I., Bryukhanov V. V. Modelling optical polarization processes on laser modified titanium with a polyvinyl alcohol film. *Condensed Matter and Interphases*. 2022;24(4): 545–558. https://doi.org/10.17308/kcmf.2022.24/10559

Для цитирования: Цибульникова А. В., Ханкаев А. А., Артамонов Д. А., Самусев И. Г., Слежкин В. А., Лятун И. И., Брюханов В. В. Моделирование оптических поляризационных процессов на лазерно-модифицированном титане с пленкой поливинилового спирта. *Конденсированные среды и межфазные границы*. 2022;24(4): 545–558. https://doi.org/10.17308/kcmf.2022.24/10559

✉ Anna V. Tsibulnikova, e-mail: anna.tsibulnikova@mail.ru

1. Introduction

Currently, femtosecond laser structuring is one of the most promising ways to modify metal surfaces at the micro and nanoscale in order to provide them with special physical and optical properties [1–3]. The formation of laser induced periodic surface structures (LIPSS) is influenced not only by the parameters of laser radiation (duration, frequency, fluence), but also by the environment in which the radiation interacts with the material [4–6]. There is a great interest in such surfaces which is explained by their unique spectral [5–7], mechanical [5, 8–10], tribological [8, 10, 11], and other physicochemical properties [8, 10–12]. The peculiarities of the creation of LIPSS make it possible to use such metamaterials in various optosensor and biophysics applications [13–17] and also as plasmon transducers of electromagnetic radiation in visible and terahertz regions [18].

It is known that surface plasmons of different mode compositions are generated on micro- and nanostructured rough metal surfaces [18–21]. In addition to the morphological parameters of the structured surface, the generation efficiency of local plasmons on the elements of roughness is greatly influenced by the medium on the surface of the material, in which the electromagnetic wave propagates and exponentially decays in a direction perpendicular to its surface. It is known that the physical reason for the generation of surface plasmons on the metal surface is the presence of an interfacial nanometre film (for example, oxide) on the metal-dielectric interface where the transformation of electromagnetic energy takes place [22, 23]. Some authors also consider layered systems consisting of metal-dielectric compounds and conductive media [24–26]. The localization regions of surface plasmons for such media can be both within the optical range and within the range of infrared frequencies [18, 23, 27]. Thus, changes in the surface morphology by introduced metal-dielectric-metal nanoparticles or resonators leads to the formation of a resonance plasmon spectrum in the IR region [27]. These structural changes mean that many parameters need to be taken into account when modelling plasmon fields and designing plasmon emitters on metasurfaces, which makes this process challenging [28–31] due to complex processes of radiation interaction and conversion on the surface of the modified material.

When metasurface is created by laser lithography, it is possible to use Pancharatnam–Berry phases of plasmon scattering [30] and create nano-optical elements and devices [32]. Thus, for example, when titanium is exposed to linear polarized femtosecond radiation, linear ablated structures of different geometric sizes shaped as strips consisting of grooves and bumps appear as a result of surface self-organisation [2, 4, 5, 16, 17]. When a metal metasurface is created by circular polarized femtosecond radiation [7, 32–34], there appears a vortex electromagnetic field leading to the formation of rotating ablated arched micro- and nanostructures which melt and solidify. Thus, nonlinear laser lithography allows creating on metal linear and "twisted" structures of different nanoroughness [35–37] with new optical elements.

The key physical problems of this work include: to use laser structuring to create ablated micro- and nanostructures on the surface of titanium by means of linear and circular radiation with a wavelength of 1 μm at different energy levels of high intensity; to record surface plasmons appearing under the influence of radiation on the rough metasurface-dielectric (micron film of polyvinyl alcohol) interface; and to study the features of their optical polarized reflectance spectra.

It should be noted that this work continues a series of works dedicated to plasmon photoprocesses on laser-structured metal surfaces with the participation of dye molecules and biological objects.

2. Experimental

The femtosecond laser structuring of the surface of a rolled titanium strip (plate) with a thickness of d ~ 0.6 mm was carried out using a TETA-25 laser system (Avesta, Russia). The laser emission parameters were as follows: the duration of a single pulse was 280 fs with a pulse repetition rate of 25 kHz. The laser operated in pulse decimation mode controlled by Lascos software. The sample (titanium plate) was shifted using a two-axis motorized positioner (Shtanda, Lithuania) controlled by

XILab software. The surface was structured by laser radiation with linear and circular polarization. Circular polarization was achieved by passing the laser beam through a CP1L1064 circular polarizer (Thorlabs, USA) placed on the laser's path between the focusing lens and the flat mirror. The laser output power was measured with an Ophir meter (Nova II, Israel).

2.1. Structuring the surface of the titanium plate

Pointwise structuring of the titanium surface was carried out as follows. The sample was placed on the motorised positioner and shifted relative to the position of the laser beam focused on the surface by a system of mirrors and lenses. When the sample was shifted, the angle between the polarization vector of the laser radiation and the direction of the sample movement was 45 degrees. The duration of the radiation exposure for a zone was between 25 and 750 ms. The distance between the centres of the zones was 100 μm, which meant that there were no overlapping zones. The power of laser radiation incident on the sample was P = 40 mW, which was sufficient to overcome the critical value necessary for titanium surface structuring [5].

This structuring method was implemented for two types of laser radiation polarization: linear and circular. Titanium linear structuring was performed at a scanning rate of 500 μm/s.

Polymer PVA films were then coated to the structured titanium surfaces.

The morphology of the titanium surface was examined using a Zeiss Cross Beam-540 (FIB-SEM) electron microscope.

2.2. Applying PVA films on the laser-structured surface of titanium

An Ossila Spin Coater (Great Britain) was used to apply PVA films on the structured surfaces of titanium. The sample was spun to the rotation speed of 6,000 rpm, and then a drop of 9% aqueous PVA solution was applied at its centre. Under the action of centrifugal force, the solution evenly distributed over the surface of the sample. The thickness of the obtained film was 750 nm.

2.3. Spectral measurements

Permittivity spectra and reflectance spectra of polarized radiation were measured using a spectral ellipsometer in the wavelength range of 450-1,000 nm (AUTO SE, Horiba-France).

3. Results and Discussion

Let us consider the effect of the type of laser radiation polarization on the LIPSS transformation under the changing duration of laser treatment.

3.1. Morphology of titanium structures obtained as a result of linear and circular polarization of laser radiation

In the first series of experiments, SEM microscopy was used to study the morphological features of the titanium surface after it was exposed to a laser beam with linear and circular polarization of various durations.

Fig. 1 shows SEM scans of the surface after it had been exposed to a set of pulses with linear polarization with the total duration of laser treatment of 25 and 100 ms (Fig. (a) and (b)) and with circular polarization with the duration of laser treatment of 25s, 100, 250 ms, and 750 ms, respectively.

The general physical processes that result in the appearance of laser-modified structures on titanium metasurfaces presented in Fig. 1 have been described in detail in [5]. This work considers these processes in terms of optical wave processes of diffraction and interference that occur on the elements of the material roughness. It also takes into account thermodynamic processes of superfast melting which result in an instantaneous change in the phase of the material [38–41].

After 25 ms of laser treatment (number of pulses N_{puls} = 625), ripple structures with connecting bridges began to form on the surface (Fig. 1a). The interval between such structures was ~1 μm. This corresponded to the wavelength of the laser radiation λ = 1,035 nm. The width of such structures corresponded to half of the wavelength and was equal to ~ 500 nm. As the laser beam penetrated deeper into the material (with an increase in the duration of treatment to 100 ms, N_{puls} = 2,500), the initial large ripple structures with a size of 500 nm transformed into smaller/more frequent structures (Fig. 1b, insert) whose width was approximately 4 times smaller. It should be noted that in the case of linear polarization, the $\boldsymbol{E}$ vector in the incident

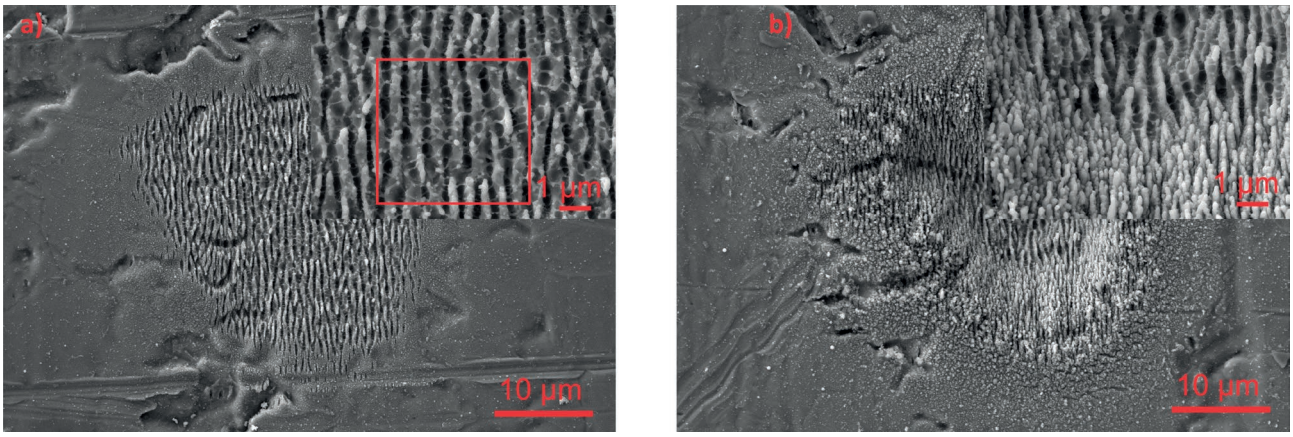

Fig. 1. SEM images of the titanium surface after femtosecond laser treatment with linear polarization of incident radiation with a total time of treatment of: a) 25 ms; b) 100 ms. Insert (a) shows a sample of ripple structures on the titanium metasurface which can serve as elements of a reflective diffraction grating

wave oscillated parallel to the plane of the sample surface. The formation of parallel ripple structures was also largely determined by the surface polarization (linearly oriented and perpendicular to the surface of the material).

At given values of the energy of laser treatment (with a total time of treatment of 25 ms), studied ripple structures on the titanium metasurface could be considered as elements of a reflective diffraction grating with the main diffraction maxima: $d \cdot \sin\varphi = k \cdot \lambda$, duration d = 770 nm at an angle $\varphi = 30°$ and a line density $N \sim 1{,}200$ mm^{-1}, and a gloss wavelength of 750 nm. This means that the ripple structures on the titanium metasurface can become good optical elements of reflective diffraction gratings used in integrated nano-optics.

The formation of such titanium metasurface structures can be described as a three-step process under both types of polarisation of incident radiation. Due to the action of an electromagnetic wave with a duration of 280 fs and an energy density in the laser pulse ($W = 0.17 \cdot 10^9$ W/m^2) sufficient to melt and evaporate the material during one femto pulse, all the energy absorbed by the material was transmitted to the crystal lattice in several steps (heating of conduction electrons and transfer of heat from electrons to the lattice, electron-phonon interaction) [35, 42–44].

Superfast (less than the duration of 1 pulse) heating of electron gas in the metal accompanied by electron-phonon relaxation led to high-temperature heating of the metal which resulted in the formation of plasma and instant (superfast) melting (less than 1 ns). The process of continuous melting of titanium lasted for 100 ms and was accompanied by a radial distribution of the material which resembled the effect of drilling followed by stretching of newly formed flat structures towards the centre. This was due to the forces of electromagnetic interaction between the charge density of molten metallic titanium. At the same time, it is known that heating titanium to 600–700 °C results in the formation of a TiO_2 oxide layer. The process of metal oxidation under the influence of laser radiation with a duration of about 1 ns and 1 fs has been well studied [34, 39]. Pulsed high-intensity laser treatment under the influence of radiation λ = 1.035 μm, leads to a change in the morphology and phase composition of the oxide film on titanium. Thus, modern studies show [45, 46] that thermally oxidised films of titanium with a thickness of 120 nm are synthesised at a temperature of 600 to 1,000°C. In this case, the structure of the film turns into rutile and takes the shape of a column and as temperature increases, the phase of the oxide film can change from amorphous to ordered (rutile, anatase). Experimental data show that long-term oxidation at temperatures of 1,000 °C leads to a transition from the parabolic to the linear law of growth of the oxide layer on the surface of titanium accompanied by the formation of pores and cracks in the formed oxide [47]. Also, it should be noted that the electronic processes in the film of titanium oxide in the UV region are caused by transitions in the band gap ($\lambda \sim 3.6$ eV)

since it is a wide-gap semiconductor material [48]. Along with these slow thermal processes resulting in the formation of titanium oxide film, the material exposed to the femtosecond laser reaches melting and evaporation temperatures of up to 2,000 °C and then cools at a high rate [3], which is followed by the precipitation of the sprayed material. This results in the metasurface roughness and dispersion of nano- and micro-adsorbed titanium nanoparticles with the oxide film. Then, the material oxidizes over a time of about 1 ns and several tens of femtoseconds. This process has been well studied [34–43, 49].

Thus, when titanium was exposed to the femtosecond laser beam, a rough metasurface with precipitated titanium and titanium oxide nanoparticles was formed. Such a surface structure exhibited special spectral and plasmonic properties, which will be described later in this paper.

It should be noted that when the surface of titanium was exposed to laser radiation with circular polarization, the same thermal processes occurred on the surface of titanium and in the material as in the case of linear polarization. However, in the case of circular polarization, the $\boldsymbol{E}$ vector followed a spiral trajectory [32, 40, 49–51], which caused the induction of electrical dipoles on the lateral extensions of the cone, What is more, the vector of dipole moments parallel to the $\boldsymbol{E}$ vector was directed to the centre of the symmetry axis of the cone.

Let us consider the spatial distribution of the ablated material on the titanium metasurface under the circular polarisation of radiation (Fig. 2).

Exposure to laser radiation with a duration of 25 ms resulted in occasional ablation from the surface layer of titanium with a TiO_2 oxide layer and local cracking of the material (Fig. 2a). It should be noted that the thickness of titanium oxide at ordinary temperature was approximately ~20 nm, which was determined by the ellipsometer resolution (AUTO SE, Horiba-France). It can be seen in the figure that islets of TiO_2 film with an average size of < 1.0 μm formed on the surface (Fig. 2a, insert). At the same time, there was almost uniform distribution of ablation cavities and metal splashes (light points) on the surface of titanium, which can be due to the uniform distribution of the photonic field in the laser beam.

With an increase in the number of pulses to 2,500 (100 ms), the laser beam went deeper into the material and the ablated material (titanium and TiO_2) distributed radially in the centre of the beam (insert, right corner of Fig. 2b). The centre of the beam formed deep cavities on the titanium surface and occasional ablated structures of different densities on the periphery. It was evident that with an increase in the energy, the fragmentation of the oxide film and cracking of the oxide layer continued.

Fig. 2d shows the region which was structured by the laser for 750 ms (~18,750 pulses) with circular polarization. As a result, a cone with a base equal to the diameter of the beam (~26 μm) was formed. From the base to the point of the cone, ablated material had distributed radially on the inner lateral surface of the cavity. An interesting effect was observed: the formation of lobed structures of metallic titanium coated with titanium oxides TiO_2 (insert, Fig. 2d [4]), which were distributed along the circles, from the base to the centre, perpendicular to the lateral surface. Such structures are sometimes called surface debris.

As the energy density of the laser beam increased, the laser-ablated spot widened (Fig. 2d), however, the pattern remained almost the same. At the same time, in comparison with the ripple structures that appeared during linear laser polarization used to form ablated titanium metasurface, in the case of circular polarization of radiation, the ablated ripple structures (surface ripple of the shock wave) changed at an angle of $\Delta\alpha \sim 15°$. The length of each nano-structure was determined by the pulse duration of the set of photons. The number of these structures on the disc of the ablated spot along the circumference and depth of the cavity was estimated (Fig. 2d – [2]). It appeared to be equal to approximately 90,000 units. This is significantly more than the number of laser pulses generated during 750 ms, which can be due to the additional vortex ablation of the material and hydrodynamic processes resulting in the formation of vortex ripple structures located along the radius of the ablation cavity, which was composed of two types of dependencies:

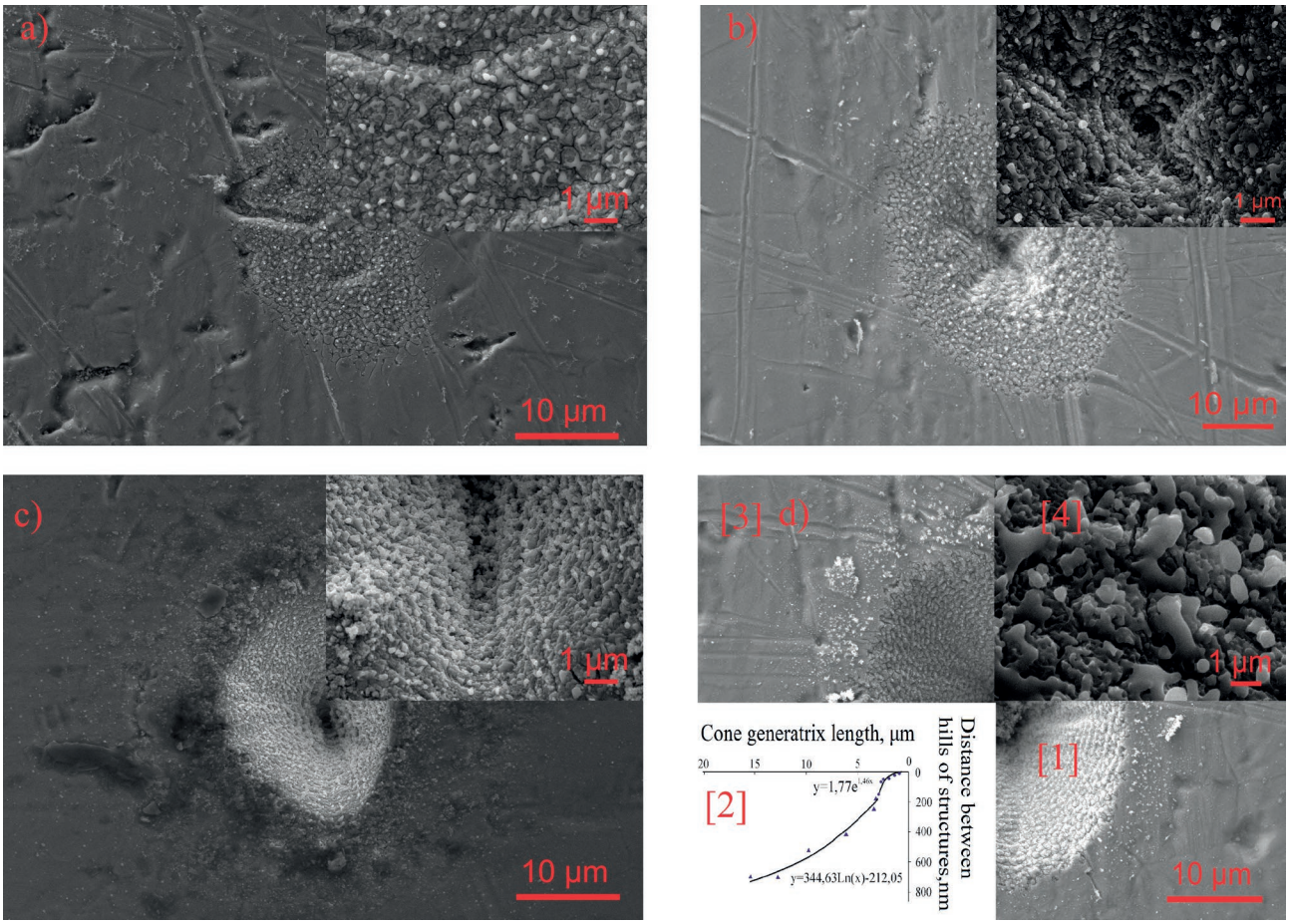

Fig. 2. SEM images of the modified titanium surface after femtosecond laser treatment with circular polarisation of incident IR radiation (λ = 1,036 nm) with a total time of treatment of: a) 25 ms; b) 100 ms; c) 250 ms; d) 750 ms. Figure 2d shows the SEM quadrants (1, 2, 3, 4) of an ablation cavity: (1) backlit; (2) graph of the function of the cavity profile; (3) surface; (4) (insertion) lobed ablated structures of 1 μm (surface debris)

$y = 344.6\,\mathrm{Ln}(x) - 212.05$

and

$y = 1.769e^{1.465x}$.

It can be assumed that the obtained logarithmic dependence reflects the combination of electron-phonon processes (t ~ 0.1 ps) and thermal processes of melting and evaporation of the material (t < 1 ns). According to the two-temperature model of titanium ablation used in our experiment, the exponential function can reflect material ablation with a high rate of material release from the cavity ("recast layer") [35, 39, 41–44].

The obtained results of the study of metal titanium ablation with circular polarisation of radiation showed that the change in the type of polarisation of the incident beam significantly changes the surface relief at the same power of treatment and with a different duration. Laser pulses with circular polarisation led to the formation of conical cavities with a radial distribution of the material along the lateral surface.

3.2. Deposition of a thin PVA film and calculation of its thickness

It was noted above that a nanometre oxide film appeared as a result of the exposure of the structured titanium metasurface to radiation. On the other hand, it is known [41] that all optical plasmon processes are generated in thin metal-dielectric structural films. It was interesting to apply a polymer film on the laser-structured titanium surface and to expose it to femtosecond laser radiation with circular polarisation. The thickness estimate is given below:

$$m_{PVA} = \omega \times m_p;\ V_{PVA} = \frac{m_{PVA}}{\rho};\ \delta = \frac{V}{S}. \quad (1)$$

Where m_{PVA} is the mass of the PVA solution, ω is the molar mass of the substance, m_p is the mass of the substance, V_{PVA} is the volume of PVA, ρ is the density of the substance, S is the area of the substrate surface, and δ is the thickness of the film.

Thus, the thickness of the PVA film on the surface of the structured titanium was d ~ 750 nm.

Optical density D of the PVA film on the glass is shown in Fig. 3. The ellipsometric method was used to determine the permittivity function of the film in the optical range from 450 to 1,000, which has constant values for functions Re(ε) ≈ 2.3 and Im(ε) ≈ 0.1.

3.3. Optical properties of Ti LIPSS after the exposure of the PVA film to circularly polarized laser radiation and simulation of spectral functions

3.3.1. Simulation of laser treatment with circular polarisation on the metasurface of titanium with PVA

Fig. 4 shows the optical spectra of the real Re(ε) and imaginary Im(ε) permittivity of titanium. The surfaces of titanium were modified in the form of cavities (Fig. 4) by means of laser structuring by sets of femto pulses (Fig. 4) with a duration of 100 ms and with circular polarization. PVA films (d ~ 750 nm) were applied to the surface structured with laser pulses within a square area of 2.25 mm²: 1.5×1.5 (Fig. 2b).

The curves in Fig. 4a correspond to the experimental and theoretical spectra of the permittivity function for the surface of structured titanium with PVA.

Let us consider the experimental curves of the permittivity function (solid curves). For example, in the spectrum of the imaginary component, maxima were observed at wavelengths of 500, 660, 780, and 815 nm. These wavelengths were characterised by the absorption of incident radiation by the surface. Let us determine the regions of plasmonic oscillations for a given surface taking into account the experimental permittivity spectrum obtained for a smooth unstructured titanium surface (Fig. 4b). It should be noted that the spectrum obtained for a smooth titanium plate corresponded to the literature

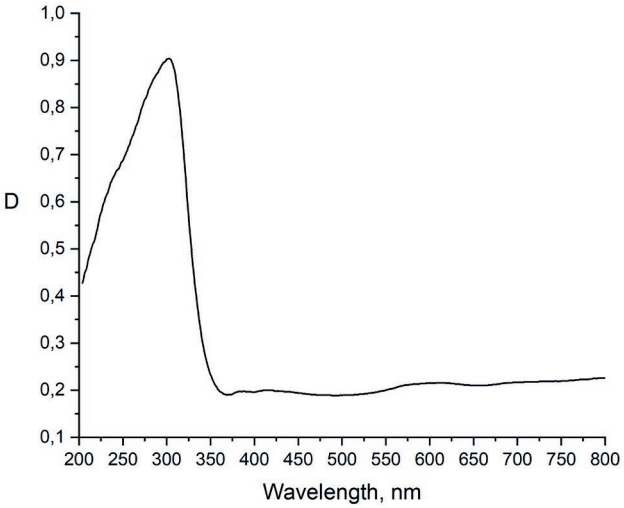

Fig. 3. Spectrum of optical density of a PVA film on silicate glass

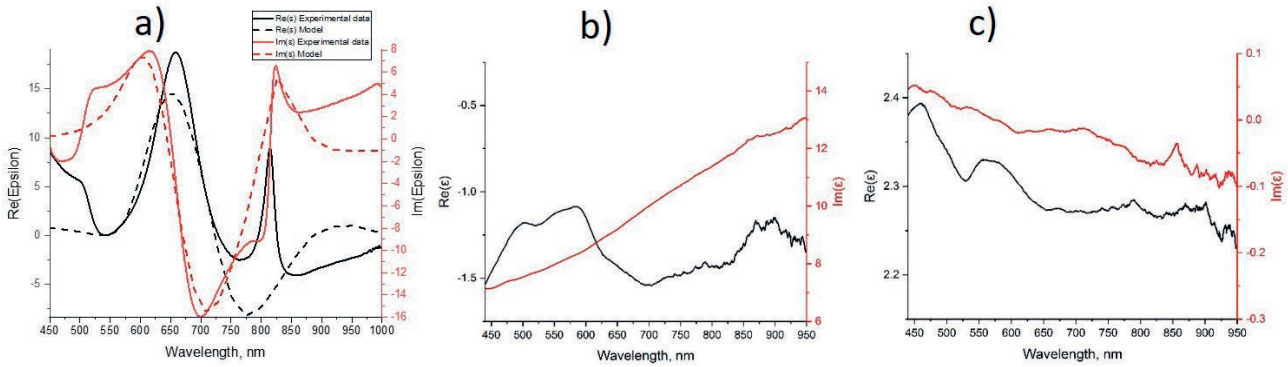

Fig. 4. Spectra of real Re(ε) and imaginary Im(ε) permittivity of titanium: (a) solid curve: experimental spectra and dotted curve: simulation for structured titanium with a PVA polymer film; (b) permittivity spectra for a smooth titanium plate; (c) permittivity spectra for a smooth titanium plate with a polymer PVA film

data presented in works [35, 47, 52] and the spectral distribution of functions confirmed to the classical Drude model for a free electron gas. For example, since maxima were present in the spectrum of negative Re(ε) permittivity component within the range of 450–700 nm, the region of possible generation of surface plasmons could be located at wavelengths of 500 nm and 600 nm. However, the range of positive values for Im(ε) (Fig. 4a) corresponded to 450–650 nm and 800–1,000 nm at these wavelengths Re(ε) ~ 0 (450–650 nm) and Re(ε) < 0 (800–1000 nm). Therefore, it can be argued that on the studied surface prepared by means of circular polarization of laser radiation, in the presence of a polymer film surface plasmons appear in the region of 500 and 600 nm. It should be noted that the unstructured titanium surface had no maxima of this kind in the presence of a polymer film and the functions of ε remained almost constant over the entire wavelength range of 450–1,000 nm (Fig. 4c). This means plasmonic oscillations are generated and propagated over the rough surface (at 500 and 600 nm) on the structure of a metal-dielectric with a thin PVA polymer film [35, 41, 44–48, 50–53].

Let us consider the low-frequency range with the maximum of the imaginary component within the region of 800 nm (Fig. 4a). For example, resonance at this wavelength may be due to volume plasmon oscillations. Here it is necessary to add that this spectrum was quite narrow with a half-width of Δλ ~ 20 nm, which may indicate high-volume and fast (τ ~ 1–2 fs) electronic processes in the metal. It should be noted that in the case of smooth titanium (Fig. 4b), there were no such maxima in the spectrum at this wavelength due to the complete screening of the incident radiation by free electrons.

To determine the contribution of various types of electrons (free and bonded) to the spectral composition of functions, curves Re(ε) and Im(ε) were simulated by means of ellipsometry. The Drude-Lorentz dispersion model was used to simulate the optical functions of the structured titanium surface with a thin-film polymer coating.

This dispersion model is a combination of the Lorentz and Drude models and it takes into account the contributions of both types of electrons [44–48, 50–54]:

$$\tilde{\varepsilon}(\omega) = \varepsilon_\infty + \frac{\omega_p^2}{-\omega^2 + i\Gamma_d\omega} + \frac{(\varepsilon_s - \varepsilon_\infty)c_t^2}{\omega_t^2 - \omega^2 + i\Gamma_0\omega} + \\ + \sum_{j=1}^{2} \frac{f_j\omega_{0j}^2}{\omega_{0j}^2 - \omega^2 + i\gamma_j\omega}, \quad (1)$$

where ε_∞ is high-frequency permittivity; ε_s is the difference between ε_s and ε_∞ which determines the force of the Lorentz oscillator; ω_t is the resonance frequency of the oscillator, whose energy corresponds to the absorption peak; Γ_0 is the attenuation coefficient of the Drude oscillator ; f_j is the force of the oscillator; ω_{0j} is resonance frequency; and γ_j is the spread-out parameter. Where ω is plasma frequency corresponding to the position of the photon energy at ε(ω) = 0; and Γ_d is the value of the resonance plasmon oscillator ($0.4 < \Gamma_d < 4$).

The parameters of the dispersion model are given in Table 1.

The spectra simulation was carried out at 121 points on a structured titanium surface with an area of 1.5×1.5 mm² in the presence of a polymer film. The average spectrum shown in Fig. 4a with dotted curves agrees well with the experimental spectra. Some differences between the value of the oscillator force f_1 = –4,308 and the theoretical value of $f_1^{theor} < 1.0$ in the Drude–Lorentz model can be due to the presence of a PVA polymer film whose dielectric properties can have a considerate influence in the blue region of the spectrum.

It should be noted that when the combined Drude–Lorentz model was used, the plasma

Table 1. Parameters of the dispersion model

ε_∞	ε_s	ω_t, eV (λ, nm)	ω_p, eV (λ, nm)	Γ_0	Γ_d	f_1	$\omega_{0.1}$, eV (λ, nm)	γ_1	f_2	$\omega_{0.2}$, eV (λ, nm)	γ_2
1.304	1.986	1.530 (784)	1.009 (1189)	0.224	7.995	-4.308	1.988 (603)	0.666	2.881	2.110 (569)	0.519

Note: Pearson correlation coefficient χ^2 for modelling is $\chi^2 = 0.000073$ and indicates the possibility of using this model to calculate experimental functions.

frequency of oscillations in the region of 600 nm (ω = 2.023) manifested as the oscillator frequency with an oscillator force of 0.104 and an attenuation factor of 0.666. This model is of some interest and can be considered as an energy-efficient characteristic of the obtained surface with a given geometry of surface structures and a dielectric film of a certain thickness. The resonance frequency in the region of 580 nm also corresponded to plasmon oscillations, however, the attenuation factor decreased to 0.519.

At the same time, the simulation allowed us to determine the average value (calculated from the 121st measurement) of the thickness of the polymer coating and to use the experimental data to draw a conclusion about the continuity of the film applied to the structured titanium surface.

This research is essential for a variety of applications. For example, ellipsometry allowed establishing that the average thickness of the polymer coating was (710 ± 20) nm, which almost coincided with the pre-calculated thickness of the PVA film (750 nm).

The results of the simulation are as follows: it was established that the spectra of surface and volume plasmons at λ = 600 and 800 nm, respectively, can be described within the framework of the proposed model. It should be noted that the experimental spectrum Re(ε) (Fig. 4a, red solid curve) had a narrow absorption maximum in the region of 815 nm due to the absorption of the PVA film. It can be assumed that this maximum appeared as a result of dipole-dipole processes of energy absorption in the PVA film, which was also observed on the smooth surface of titanium with PVA (Fig. 4c, red solid curve). During simulation, this maximum shifted to the IR region and was a wide spectrum with a half-width of ~200 nm. The obtained spectral difference can be explained by the fact that when modelling functions, it is difficult to take into account the physical and chemical parameters of the polymer coating (molecular structure, solubility of polymer globules). However, film thickness and optical density were taken into account.

3.3.2. Reflectance coefficients of s- and p-polarized light from the metasurface of titanium with PVA

It was of interest to study the optical reflectance spectra of linearly polarized laser radiation from the metasurface of titanium with a PVA film (Fig. 5) pre-treated with circularly polarized laser radiation within the range of 450–1,000 nm.

The reflectance coefficients of *s*- and *p*-polarized radiation of the structured titanium surface are shown in Fig. 5a. It was shown that these functions had their minima in the region of 450–500 nm and 815 nm. These wavelengths coincided with the regions shown in Fig. 4a, which

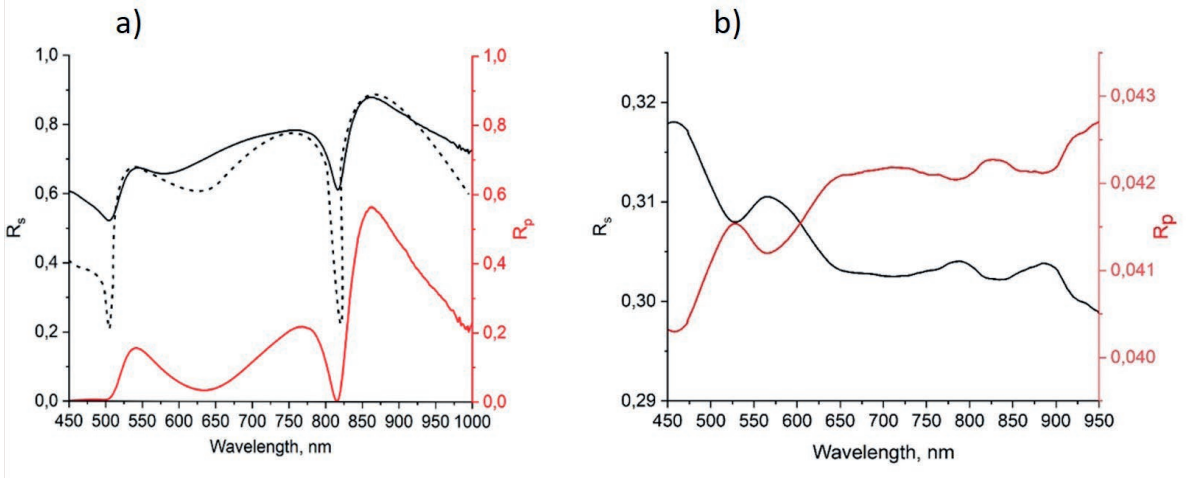

Fig. 5. (a) Reflectance coefficients of *s*- and *p*-polarised light from the structured surface with a PVA film (solid curves) and the reflectance spectrum of s-polarised light obtained by simulation according to formula (1), with a PVA film (black dotted curve). (b) Reflectance coefficients of *s*- and *p*-polarised light from unstructured surface with a PVA film (solid curves)

confirms the hypothesis about the generation of surface plasmons in this wavelength range. At the same time, it was *p*-polarized radiation that contributed more since it was absorbed more than *s*-component. This indicates that for *p*-polarized light, the difference between the values of the reflectance coefficients in their local minima is close to zero, and at these points the surface is almost mirror. What is more, for s-polarised radiation, the reflectance coefficients from the surface had rather large values of 0.52 and 0.58 for wavelengths of 500 and 815 nm, respectively. It should be noted that the spectral analysis shown in Fig. 4a and Fig. 5a revealed more significant differences in the position of the spectral maxima in the red region of the visible range at wavelengths of 650–850 nm. This may be due to the polarizing properties of the polymer film, which requires additional optical experiments to estimate the optical density of the PVA film based on its thickness.

In the case of reflection of *s*-polarized radiation, the simulation of the reflection processes of the titanium metasurface was performed according to the Fresnel equations [45, 48, 49]:

$$R_s^F = \left|r_s^F\right|^2, r_s^F = \frac{\left(\frac{\omega^2}{c^2}\varepsilon_1 - k_\parallel^2\right)^{1/2} - \left(\frac{\omega^2}{c^2}\varepsilon_2 - k_\parallel^2\right)^{1/2}}{\left(\frac{\omega^2}{c^2}\varepsilon_1 - k_\parallel^2\right)^{1/2} + \left(\frac{\omega^2}{c^2}\varepsilon_2 - k_\parallel^2\right)^{1/2}},$$

$$P_{SP} = k_\parallel^2 = \frac{\omega^2}{c^2}\frac{\varepsilon_1\varepsilon_2}{\varepsilon_1 + \varepsilon_2}.$$

Where $\varepsilon_1, \varepsilon_2$ is the permittivity of the metal and the plasmon propagation medium, respectively, ω is the frequency of external radiation, c is the speed of light; and $k_{||}$ is the wave vector of plasmons.

The results of comparing experimental and modelling reflectance coefficients according to the above mentioned formulas are shown in Fig. 5a. It is obvious that experimental and theoretical data have extremes at the same wavelengths. However, it is worth noting that the values of the reflectance coefficients in their minimums do not coincide. Thus, it was shown that the minima model value of the reflectance coefficient of *s*-polarized light was ~0.2 while according to the experimental data the reflectance coefficient had a value of ~0.5.

It should be noted that the reflectance coefficients of *s*- and *p*-polarized radiation reflected from the unstructured titanium surface (smooth titanium, Fig. 5b) with a PVA film significantly differed in values in the wavelength range of 450–1,000 nm and were equal to $R_S = 0.33$ and $R_P = 0.04$.

4. Conclusions

Smooth titanium plates were structured by femtosecond laser treatment with linear and circular polarization with a wavelength of λ = 1.035 μm and a total time of treatment of: t_i = 25, 100, 250, and 750 ms and the duration of τ = 280 fs. This resulted in occasional ablation of the material and the formation of cavities <1.0 μm in size and a repeated layer with surface ripples caused by the shock wave.

Spectral permittivity functions during plasmon generation were simulated for the titanium metasurface with a PVA film (750 nm thick).

When titanium plates were exposed to laser radiation with circular polarisation and different energy, ripple structures and cavities appeared following a completely different optical pattern. Thus, for example, exposure to a circular field resulted in the formation of cone-shaped loped cavities and circular ripple nano- and microstructures along the line of action of laser beam pulses.

The functions (logarithmic and exponential) of laser ablation of the material and their dependence on energy were studied along the lateral surface of cavities formed as a result of electron-phononic and thermal processes associated with laser treatment. When modelling plasmonic processes on the metasurface of titanium with PVA, it was established that spectral parameters almost fully matched with small offsets of spectra maxima of the real Re(ε) and imaginary Im(ε) permittivities. What is more, spectral shifts of less than < 20 nm were mostly associated with the presence of a polymer PVA film on the titanium metasurface. Plasmonic processes of reflection of polarised light with R_S and R_P components from the titanium metasurface

after it was treated with circular radiation were modelled. It was found that the amplitude of the R_P polarized radiation was significantly smaller than that of the R_S component and at some points on the surface its spectral values were close to zero. It should be noted that the reflectance coefficients of R_S and R_P polarized radiation reflected from the unstructured titanium surface (smooth titanium) with a PVA film differed significantly in values within the wavelength range of 450–1,000 nm and were equal to $R_S = 0.33$ and $R_P = 0.04$.

At the same time, it was established that linear-polarized radiation during a pointwise scanning of the titanium surface with a step of 100 μm can be used to create ripple structures with a line density of $N \sim 1{,}200$ mm^{-1} and a gloss wavelength of the reflected radiation of 750 nm, which can be of great practical importance in the field of creating diffractive elements in integrated optics.

Author contributions

Conceptualisation: V. Bryukhanov; methodology: V. Slezhkin; software: A. Khankaev; formal analysis: V. Slezhkin; research: A. Khankaev and D. Artamonov; writing the article, preparation of the initial project: V. Bryukhanov; review: A. Tsibulnikova; visualisation: I. Lyatun and A. Khankaev; management: V. Bryukhanov; administration and financing of the project: I. Samusev.

Conflict of interests

The authors declare that they have no known competing financial interests or personal relationships that could have influenced the work reported in this paper.

References

1. Yu X., Zhang Q., Qi D., Tang S., Dai S., Zhang P., Xu Y., Shen X. Femtosecond laser-induced large area of periodic structures on chalcogenide glass via twice laser direct-writing scanning process. *Optics & Laser Technology*. 2020;124: 105977. https://doi.org/10.1016/j.optlastec.2019.105977

2. Messaddeq S. H., Vallée R., Soucy P., Bernier M., El-Amraoui M., Messaddeq Y. Self-organized periodic structures on Ge-S based chalcogenide glass induced by femtosecond laser irradiation. *Optics Express*. 2012;20(28): 29882–29889. https://doi.org/10.1364/OE.20.029882

3. Lim H. U., Kang J., Guo C., Hwang T. Y. Femtosecond laser-induced dual periodic structures on Ni. *Frontiers in Optics*. 2017. Washington, D.C.: OSA; 2017. https://doi.org/10.1364/FIO.2017.JTu3A.41

4. Simões J. G. A. B., Riva R., Miyakawa W. High-speed laser-induced periodic surface structures (LIPSS) generation on stainless steel surface using a nanosecond pulsed laser. *Surface and Coatings Technology*. 2018;344: 423–32. https://doi.org/10.1016/j.surfcoat.2018.03.052

5. Bonse J, Kirner S V., Krüger J. Laser-induced periodic surface structures (LIPSS). In: *Handbook of laser micro- and nano-engineering*. Springer Nature; 2020. pp. 1–59. https://doi.org/10.1007/978-3-319-69537-2_17-2

6. Lorenz P., Zagoranskiy I., Ehrhardt M., Zimmer K. P. Laser-induced large area sub-μm and nanostructuring of dielectric surfaces and thin metal layer. In: *Proc. SPIE 10906, Laser-based Micro- and Nanoprocessing XIII, 109060T, 4 March 2019*. https://doi.org/10.1117/12.2510206

7. Silvennoinen M., Hasoň S., Silvennoinen R. Optical resonance on LIPSS sensed by polarized light. In: *Proc. SPIE 9066, Eleventh International Conference on Correlation Optics, 90660X, 17 December 2013*. https://doi.org/10.1117/12.2047104

8. Rathmann L., Beste L. H., Radel T. Laser based process chain to use LIPSS on forming tools. *Surface and Coatings Technology*. 2021;426: 127761. https://doi.org/10.1016/j.surfcoat.2021.127761

9. Romano J. M., Garcia-Girón A., Penchev P., Dimov S. S. Durability and wear resistance of LIPSS. In: *Proc. Volume 11674, Laser-based Micro- and Nanoprocessing XV; 116740N*. 2021. p. 19. https://doi.org/10.1117/12.2584010

10. Karkantonis T., Gaddam A., See T. L., Joshi S. S., Dimov S. Femtosecond laser-induced sub-micron and multi-scale topographies for durable lubricant impregnated surfaces for food packaging applications. *Surface and Coatings Technology* 2020;399: 126166. https://doi.org/10.1016/j.surfcoat.2020.126166

11. Gazizova M. Y., Smirnov N. A., Kudryashov S. I., ... Prokopenko N. A. Correlation of the tribological properties of LIPSS on TiN surface with 3D parameters of roughness. *IOP Conference Series: Materials Science and Engineering*. 2021;1014(1): 012014. https://doi.org/10.1088/1757-899X/1014/1/012014

12. Exir H., Weck A. Mechanism of superhydrophilic to superhydrophobic transition of femtosecond laser-induced periodic surface structures on titanium. *Surface and Coatings Technology* 2019;378: 124931. https://doi.org/10.1016/j.surfcoat.2019.124931

13. Orazi L., Pelaccia R., Mishchenko O., Reggiani B., Pogorielov M. Fast LIPSS based texturing process of dental implants with complex geometries.

CIRP Annals. 2020;69(1): 233–236. https://doi.org/10.1016/j.cirp.2020.04.065

14. Orazi L., Pogorielov M., Deineka V., ... Reggiani B. Osteoblast cell response to LIPSS-modified Ti-implants. *Key Engineering Materials*. 2019;813: 322–327. https://doi.org/10.4028/www.scientific.net/KEM.813.322

15. Khorkov K. S., Kochuev D. A., Dzus M. A., Prokoshev V. G. Wettability surface control on stainless steel by LIPSS formation. *Journal of Physics: Conference Series*. 2021;1822(1): 012010. https://doi.org/10.1088/1742-6596/1822/1/012010

16. Zyubin A., Kon I., Tcibulnikova A., ... Demin M. Numerical FDTD-based simulations and Raman experiments of femtosecond LIPSS. *Optics Express*. 2021;29(3): 4547–4558. https://doi.org/10.1364/oe.413460

17. Vorobyev A. Y., Guo C. Femtosecond laser nanostructuring of metals. *Optics Express*. 2006;14(6): 2164. https://doi.org/10.1364/OE.14.002164

18. Zhang W., Cue N., Yoo K. M. Emission linewidth of laser action in random gain media. *Optics Letters*. 1995;20(9): 961. https://doi.org/10.1364/OL.20.000961

19. Drachev V. P., Chettiar U. K., Kildishev A. V., Yuan H.-K., Cai W., Shalaev V. M. The Ag dielectric function in plasmonic metamaterials. *Optics Express*. 2008;16; 1186–1195. https://doi.org/10.1364/OE.16.001186

20. De Sio L., Placido T., Comparelli R., ... Bunninge T. J. Next-generation thermo-plasmonic technologies and plasmonic nanoparticles in optoelectronics. *Progress in Quantum Electronics*. 2015;41: 23–70. https://doi.org/10.1016/j.pquantelec.2015.03.001

21. Chauhan M., Kumar Singh V. Review on recent experimental SPR/LSPR based fiber optic analyte sensors. *Optical Fiber Technology*. 2021; 64. https://doi.org/10.1016/j.yofte.2021.102580

22. Misra S., Zhang D., Qi Z., ... Wang H. Morphology control of self-assembled three-phase Au-$BaTiO_3$-ZnO hybrid metamaterial for tunable optical properties. *Crystal Growth and Design*. 2020;20(9): 6101–8. https://doi.org/10.1021/acs.cgd.0c00801

23. Jia X., Wang X. Optical fishnet metamaterial with negative, zero, positive refractive index and nearly perfect absorption behavior at different frequencies. *Optik*. 2019;182: 464–468. https://doi.org/10.1016/j.ijleo.2019.01.066

24. Kim J., Han K., Hahn J. W. Selective dual-band metamaterial perfect absorber for infrared stealth technology. *Scientific Reports*. 2017;7(1): 6740. https://doi.org/10.1038/s41598-017-06749-0

25. Pralle M. U., Moelders N., McNeal M. P., Puscasu I., Greenwald A. C., Daly J. T., Johnson E. A. Photonic crystal enhanced narrow-band infrared emitters. *Applied Physics Letters*. 2002;81(25): 4685–4687. https://doi.org/10.1063/1.1526919

26. Sikdar D., Pendry J. B., Kornyshev A. A. Nanoparticle meta-grid for enhanced light extraction from light-emitting devices. *Light: Science and Applications*. 2020;9(1): 1–11. http://dx.doi.org/10.1038/s41377-020-00357-w

27. Naik G. V., Kim J., Boltasseva A. Oxides and nitrides as alternative plasmonic materials in the optical range. *Optical Materials Express*. 2011;1(6): 1090. https://doi.org/10.1364/OME.1.001090

28. Sakurai A., Bo Z., Zhang Z. Prediction of the resonance condition of metamaterial emitters and absorbers using LC circuit model. In: *International Heat Transfer Conference 15, August, 10-15, 2014, Kyoto, Japan*. 2014. pp. 7067–7076. https://doi.org/10.1615/IHTC15.rad.009012

29. Wei D., Hu C., Chen M., ... Xie C. Optical modulator based on the coupling effect of different surface plasmon modes excited on the metasurface. *Optical Materials Expres.s* 2020;10(1): 105–118. https://doi.org/10.1364/ome.382116

30. Tao H., Bingham C. M., Strikwerda A. C., ... Averitt R. D. Highly flexible wide angle of incidence terahertz metamaterial absorber: Design, fabrication, and characterization. *Physical Review B – Condensed Matter and Materials Physics*. 2008;78: 241103. https://doi.org/10.1103/PhysRevB.78.241103

31. Alves F., Kearney B., Grbovic D., Karunasiri G. Narrowband terahertz emitters using metamaterial films. *Optics Express*. 2012;20(19): 21025–21032. https://doi.org/10.1364/OE.20.021025

32. Lazzini G., Romoli L., Tantussi F., Fuso F. Nanostructure patterns on stainless-steel upon ultrafast laser ablation with circular polarization. *Optics and Laser Technology*. 2018;107: 435–442. https://doi.org/10.1016/j.optlastec.2018.06.023

33. Khorasaninejad M., Chen W. T., Devlin R. C., Oh J., Zhu A. Y., Capasso F. Metalenses at visible wavelengths: Diffraction-limited focusing and subwavelength resolution imaging. *Science*. 2016;352(6290): 1190–1194. https://doi.org/10.1126/science.aaf6644

34. Öktem B., Pavlov I., Ilday S., Kalaycıoğlu H., Rybak A., Yavaş S., Erdoğan M., Ömer F. Nonlinear laser lithography for indefinitely large-area nanostructuring with femtosecond pulses. *Nature Photonics*. 2013;7(11): 897–901. https://doi.org/10.1038/nphoton.2013.272

35. Dostovalov A. V., Korolkov V. P., Babin S. A. Formation of thermochemical laser-induced periodic surface structures on Ti films by a femtosecond IR Gaussian beam: regimes, limiting factors, and optical properties. *Applied Physics B: Lasers and Optics*. 2017;123: 30. https://doi.org/10.1007/s00340-016-6600-z

36. Emmony D. C., Howson R. P., Willis L. J. Laser mirror damage in germanium at 10.6 μm. *Applied*

Physics Letters. 1973;23(11): 598–600. https://doi.org/10.1063/1.1654761

37. Sipe J. E., Young J. F., Preston J. S., van Driel H. M. Laser-induced periodic surface structure. I. Theory. *Physical Review B*. 1983;27(2): 1141–1154. https://doi.org/10.1103/PhysRevB.27.1141

38. Maier S. A. *Plasmonics: fundamentals and applications*. New York: Springer; 2007. https://doi.org/10.1007/0-387-37825-1

Klimov V. V. *Nanoplasmonics**. Moscow: Physmathlit Publ.; 2009. 115 p. (In Russ.)

40. Inouye H., Tanaka K., Tanahashi I., Hirao K. *Ultrafast dynamics of nonequilibrium electrons in a gold nanoparticle system*. *Physical Review B*. 1998;57: 11334–11340. https://doi.org/10.1103/PhysRevB.57.11334

41. Grua P., Morreeuw P., Bercegol H., Jonusauskas G., Vallée F. Electron kinetics and emission for metal nanoparticles exposed to intense laser pulses. *Physical Review B – Condensed Matter and Materials Physics*. 2003;68(12): 035424. https://doi.org/10.1103/PhysRevB.68.035424

42. Agranovich V. M., Mills D. L. *Modern problems in condensed matter sciences*. Amsterdam: North-Holland Publishing Company; 1982. pp. 3–717. https://doi.org/10.1016/B978-0-444-86165-8.50001-3

43. Brodskii A. M., M. I. Urbakh. Optics of rough surfaces of metals. *Sov. Phys. JETP*. 1985;62(2): 391–399. Available at: http://jetp.ras.ru/cgi-bin/dn/e_062_02_0391.pdf

44. Anisimov S. I., Luk'yanchuk B. S. Selected problems of laser ablation theory. *Physics-Uspekhi* 2002;45(3): 293–324. https://doi.org/10.1070/PU2002v045n03ABEH000966

45. Gerasimenko Yu. V., Logacheva V. A., Khoviv A. M. Synthesis and properties of titanium dioxide thin films. *Condensed Matter and Interphases*. 2010;12(2): 113–118. (In Russ., abstract in Eng.). Available at: https://www.elibrary.ru/item.asp?id=15176043

46. Hou Y. Q., Zhuang D. M., Zhang G., Zhao M., Wu M. S. Influence of annealing temperature on the properties of titanium oxide thin film. *Applied Surface Science*. 2003;218(1–4): 98–106. https://doi.org/10.1016/S0169-4332(03)00569-5

47. Makarov E. S., Kuznetsov M. L. The crystal structure and chemical character of lower oxides of titanium $TiO_{0-0.48}$. *Journal of Structural Chemistry*. 1960;1: 156–162. https://doi.org/10.1007/BF00738933

48. Chibisov A. N., Bizyuk A. O. Electronic structure of titanium dioxide nanoparticles*. *Vestnik Amurskogo gosudarstvennogo universiteta*. 2008;(43): 22–23. (In Russ.). Available at: https://www.elibrary.ru/item.asp?id=19007690

49. *Surface enhanced raman scattering*. R. Chang, T. Furtak (eds.). New York and London: Springer; 1982. https://doi.org/10.1007/978-1-4615-9257-0

50. Gräf S., Müller F. A. Polarisation-dependent generation of fs-laser induced periodic surface structures. *Applied Surface Science*. 2015;331: 150–155. https://doi.org/10.1016/j.apsusc.2015.01.056

51. Kang M., Chen J., Wang X. L., Wang H. T. Twisted vector field from an inhomogeneous and anisotropic metamaterial. *Journal of the Optical Society of America B*. 2012;29(4). 572–576. https://doi.org/10.1364/JOSAB.29.000572

52. Bäuerle D. *Laser processing and chemistry*. Berlin, Heidelberg: Springer Berlin Heidelberg; 1996. 279 p. https://doi.org/10.1007/978-3-662-03253-4

53. Ford G. W., Weber W. H. Electromagnetic interactions of molecules with metal surfaces. *Physics Reports*. 1984;113(4): 195–287. https://doi.org/10.1016/0370-1573(84)90098-X

54. Rosenberg H. M. *The solid state : an introduction to the physics of solids for students of physics, materials science, and engineering*. Oxford University Press; 1992. 315 p.

Информация об авторах

Anna V. Tsibulnikova, Cand. Sci. (Phys.–Math.), Senior Researcher of REC "Fundamental and applied photonics. Nanophotonics", Immanuel Kant Baltic Federal University (Kaliningrad, Russian Federation).

https://orcid.org/0000-0001-8578-0701

anna.tsibulnikova@mail.ru

Artemii A. Khankaev, postgraduate student, technician of REC "Fundamental and applied photonics. Nanophotonics", Immanuel Kant Baltic Federal University (Kaliningrad, Russian Federation).

https://orcid.org/0000-0003-0661-5228

akhankaev@gmail.com

Dmitry A. Artamonov, postgraduate student, technician of REC "Fundamental and applied photonics. Nanophotonics", Immanuel Kant Baltic Federal University (Kaliningrad, Russian Federation).

euroset2016ig98@icloud.com

Ilya G. Samusev, Cand. Sci. (Phys.–Math.), Deputy Vice-Rector for Research, Head of R&D Department, Director of REC "Fundamental and applied photonics. Nanophotonics", Immanuel Kant Baltic Federal University (Kaliningrad, Russian Federation).

https://orcid.org/0000-0001-5026-7510

is.cranz@gmail.com

Vasily A. Slezhkin, Cand. Sci. (Chem.), Associate Professor, Kaliningrad State Technical University (Kaliningrad, Russian Federation).
https://orcid.org/0000-0002-2801-7029
vasiliy.slezhkin@klgtu.ru

Ivan I. Lyatun, Researcher, Laboratory of X-ray Coherent Optics, Immanuel Kant Baltic Federal University (Kaliningrad, Russian Federation).
https://orcid.org/0000-0002-4988-8077
ILyatun@kantiana.ru

Valery V. Bryukhanov, Dr. Sci. (Phys.–Math.), Leading Researcher, Research Center "Fundamental and Applied Photonics. Nanophotonics", Immanuel Kant Baltic Federal University (Kaliningrad, Russian Federation).
https://orcid.org/0000-0003-4689-7207
bryukhanov_v.v@mail.ru

Received 24.04.2022; approved after reviewing 17.08.2022; accepted for publication 15.09.2022; published online 25.12.2022.

Translated by Irina Charychanskaya
Edited and proofread by Simon Cox